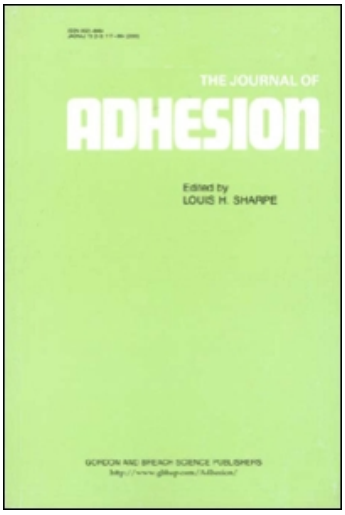

The Journal of Adhesion
Publication details, including instructions for authors and subscription information:
http://www.informaworld.com/smpp/title~content=t713453635

CONTACT ANGLE DETERMINATION OF NANOPARTICLES: REAL EXPERIMENTS AND COMPUTER SIMULATIONS

A. Agod[a]; A. Deák[a]; E. Hild[a]; Z. Hórvölgyi[a]; E. Kálmán[b]; Gy. Tolnai[b]; A. L. Kovács[c]
[a] Budapest University of Technology and Economics, Department of Physical Chemistry, Budapest, Hungary [b] Department of Nanostructures and Surface Modification, Budapest, Hungary [c] Cell Physiology Laboratory, Budapest, Hungary

Online publication date: 10 August 2010

To cite this Article Agod, A. , Deák, A. , Hild, E. , Hórvölgyi, Z. , Kálmán, E. , Tolnai, Gy. and Kovács, A. L.(2004) 'CONTACT ANGLE DETERMINATION OF NANOPARTICLES: REAL EXPERIMENTS AND COMPUTER SIMULATIONS', The Journal of Adhesion, 80: 10, 1055 — 1072
To link to this Article: DOI: 10.1080/00218460490509381
URL: http://dx.doi.org/10.1080/00218460490509381

The Journal of Adhesion, 80: 1055–1072, 2004

ISSN: 0021-8464 print/1545-5823 online
DOI: 10.1080/00218460490509381

Taylor & Francis
Taylor & Francis Group

CONTACT ANGLE DETERMINATION OF NANOPARTICLES: REAL EXPERIMENTS AND COMPUTER SIMULATIONS

A. Agod
A. Deák
E. Hild
Z. Hórvölgyi
Budapest University of Technology and Economics,
Department of Physical Chemistry, Budapest, Hungary

E. Kálmán
Gy. Tolnai
Department of Nanostructures and Surface Modification,
CRC HAS, Budapest, Hungary

A. L. Kovács
Loránd Eötvös University, Department of General Zoology,
Cell Physiology Laboratory, Budapest, Hungary

Monolayers of Stöber-silica nanoparticles (ca. 40 nm diameters) at the water–air interface have been studied in a Wilhelmy film balance. Scanning angle reflectometry and molecular dynamics computer simulation have been used to assess the contact angles of the particles. Our results indicate that the traditional film balance method of contact angle determination overestimates the real contact angles even in the lower range of particle hydrophobicities.

Keywords: Contact angle; Nanoparticles; Scanning angle reflectometry; Film balance; Computer simulation

Received 29 January 2004; in final form 29 June 2004.

This work was supported by the Hungarian Scientific Research Fund (OTKA T037643).

One of a collection of papers honoring A. W. Neumann, the recipient in February 2004 of *The Adhesion Society Award for Excellence in Adhesion Science, Sponsored by 3M*.

Address correspondence to Zoltán Hórvölgyi, Budapest Universtiy of Technology and Economics, Department of Physical Chemistry, Budapest, H-1525, Hungary. E-mail: zhorvolgyi@mail.bme.hu

INTRODUCTION

The wetting behaviour of fine particles is of great importance in numerous technological processes including froth flotation, demulsification, antifoaming procedures [1–4], and coal industries [5, 6]. Moreover, nanoparticles with special surface properties were proven to be suitable to prepare well-packed nanolayers that give an entry to the fabrication of advanced materials [7–10]. Hence, the characterization of wetting properties of particles (by contact angles) has attracted significant attention for a long time [11–26].

Contact angles of nano- and microparticles can be determined by the film balance technique [19, 27] According to this traditional method, contact angles can be calculated from the surface pressure (Π) *versus* surface area (A) isotherms of monoparticulate layers using Langmuir or Wilhelmy film balances. It is widely accepted that the measurable ("effective") surface tension (or surface pressure) can be related to the work necessary for the compression of (nano- or micro-) particulate layers and for particle removal from the liquid–gas interface [19, 25, 27]. Although in certain cases the measurements, provided useful information about the particle–particle and particle–subphase interactions [7, 19, 20, 25, 27], several questions remained unanswered. Using Langmuir and Wilhelmy film balances, it was found that there was not satisfactory agreement between the calculated (from Π-A isotherms) and the measured (directly on the beads) contact angles of medium hydrophobicity range for relatively large, spherical model particles (diameter: 75 μm) [20, 28]. Similar model investigations cannot be carried out for nanoparticles due to the extremely small particle sizes.

The main purpose of this work is to study the wettability of silica nanoparticles (*ca*. 40 nm diameters) at the water–air interface in the range of low hydrophobicities. The results obtained by the traditional film balance technique will be compared to the results of a laser optical method, scanning angle reflectometry (SAR), which has not yet been used for wettability investigations. Computer simulations of the film balance experiments are also accomplished in order to calculate the surface pressure–surface area isotherms and to compare them with the real ones that also allows us to assess the contact angles.

In this article we give a short description of the applied methods and model materials used.

THEORETICAL BACKGROUND OF THE APPLIED METHODS

Determination of Contact Angles from Surface Pressure *versus* Surface Area Isotherms

The traditional film balance method for the determination of contact angles of monodisperse spheres at the water–air interface can be applied by using the following relationship, provided, that the layer is noncohesive [27]:

$$\gamma_{WA} R^2 \pi (1 - \cos(\Theta))^2 = V^*_{rep} + \Pi_c A^*_c, \quad (1)$$

where γ_{WA} is the water–air surface tension, R is the radius of the particles, Θ is the contact angle, Π_c is the collapse pressure, A^*_c is the collapse area given for an individual particle, and π is the geometric constant. V^*_{rep}, the repulsive potential energy normalized for one particle, is proportional to the I area, and $\Pi_c A^*_c$ is proportional to the II area in Figure 1. The sum of V^*_{rep} and $\Pi_c A^*_c$ is considered as the adhesion energy of one particle if the particle is removed from the interface into the water phase during the collapse. In our opinion, the second stage (II) of the π-A isotherm (in case of non-hexagonal ordering and/or polydisperse particles, *i.e.,* if the particles have different potential energy during the compression (Figure 2) [29]) includes

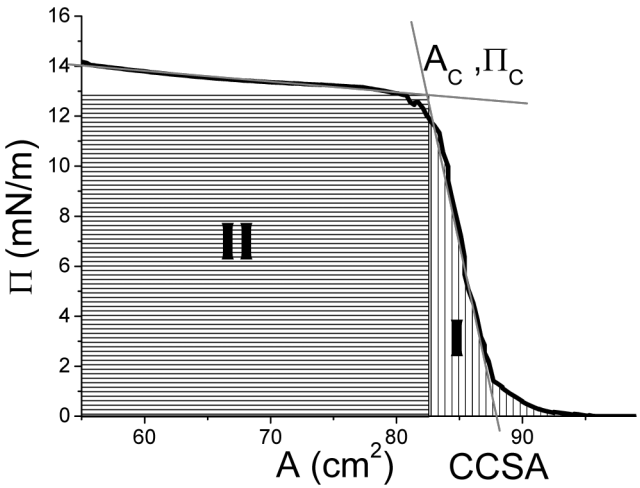

FIGURE 1 Experimentally obtained surface pressure (Π, surface area (A) isotherm; CCSA, contact cross-sectional area; Π_c, collapse pressure; A_c, collapse area.

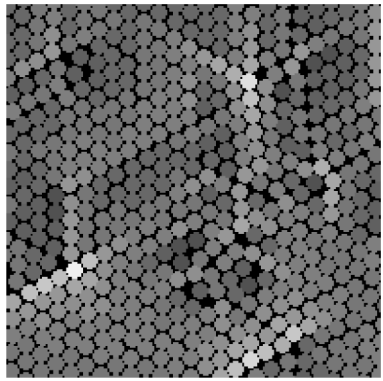

FIGURE 2 Potential energy map of particles. The darker the particles the lower the potential energies. The particles with higher potential energy are always situated at the boundaries of the hexagonally ordered domains and at the lattice defects.

not only the energy related to the particles' removal but an extra energy dissipation that relates to the continuous particle removal.

Determination of the Contact Angle by Scanning Angle Reflectometry

Scanning angle reflectometry (SAR) together with Brewster angle microscopy (BAM) [30, 31] are powerful tools for the investigation of very thin layers of nanoparticles deposited or spread on the surface of a bulk material. Both reflectance methods are nondestructive and can be applied *in situ*. They also can be realized by the same optical setup. They use the special property of *p*-polarized light waves—that the reflectance of a perfectly abrupt, smooth interface between the medium of incidence and a semi-infinite bulk is zero at the Brewster angle. Any deviation of abruptness, a rough interface or an interfacial layer, increases the reflectance. Scanning angle reflectometry, on the other hand, measures reflectivity as a function of the angle of incidence, $R(\theta)$, near the Brewster angle. The reflectance curves are compared with that of the clean surface, which exhibits a minimum; this minimum shifts, and the minimum reflectance increases, if an interfacial layer is present. Even layers of a few tens of nanometers thickness cause well-detectable change in the shape of the $R(\theta)$ curves.

The question is how to extract reliable information about the structure of an interfacial layer formed by nanoparticles, and about

the particles themselves, from the reflectance measurements. The simplest method of evaluation is when one approximates the interface between the two phases with a homogeneous (uniform) layer and finds the effective refractive index and thickness that corresponds most closely to the measured reflectance curve. This *uniform layer approach* is valid if the particles are small compared with the wavelength and their refractive index does not differ much from that of the host material [32]. For particles of size comparable with the wavelength, the light scattering must be taken into account [33].

Reflectance in the Uniform Layer Model

Assume a layer of thickness, l, and refractive index, n_1, between air and a semi-infinite substrate with refractive index, n_0 and n_2, respectively. R, the reflectance for a p-polarized light beam of wavelength, λ, and angle of incidence, θ, can be determined from the Fresnel reflectance coefficients of the interfaces r_{01} and r_{12}:

$$r_{ik} = \frac{q_i - q_k}{q_i + q_k}, \text{ with } q_i = \frac{\sqrt{n_i^2 - n_0^2 \sin^2(\theta)}}{n_i^2}, \tag{2a}$$

and from the phase change in the layer δ,

$$\delta = 2\pi \cdot l/\lambda \cdot \sqrt{n_i^2 - n_0^2 \sin^2(\theta)}, \tag{2b}$$

as

$$R = \frac{r_{01}^2 + r_{12}^2 + 2r_{01}r_{12}\cos(2\delta)}{1 + r_{01}^2 r_{12}^2 + 2r_{01}^2 r_{12}^2 \cos(2\delta)}. \tag{2c}$$

The reflectance of the uncovered substrate is $R_s = {r_{02}}^2$. This is zero at the Brewster angle of the substrate material,

$$\theta_B = \arctan(n_2/n_0). \tag{3}$$

The reflectance curves intersect the curve of the substrate at a certain angle, the Brewster angle of the layer material, θ_L (Figure 3), where the reflection coefficient of the air-layer interface vanishes; $r_{01} = 0$. This fact offers a simple tool to estimate the effective refractive index of the layer [34], n_{eff}:

$$n_{eff} = n_0 \tan(\theta_L). \tag{4}$$

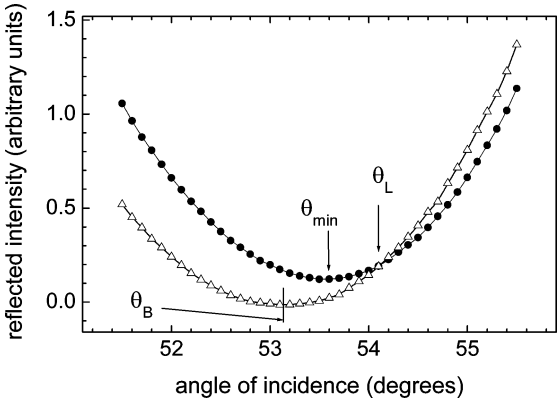

FIGURE 3 Typical measured reflectance curves: reflected intensity *versus* angle of incidence both for water and spread layer. θ_B is the Brewster angle of the water substrate; θ_L is the same for the layer. In the frames of the homogeneous model, n_{eff} and l can be obtained by a fitting procedure, but n_{eff} can be calculated also from the intersection of the two curves ($n_{eff} = tan\,\theta_L$), and the thickness can be estimated from the position of minimal reflectance, θ_{min}.

Estimation of the Average Refractive Index of a Monolayer of Spherical Particles [35]

We constructed a simplified model for the monolayer of silica particles, shown in (Figure 4). The particles are assumed spherical, of uniform size, and arranged hexagonally at the air−water interface. The silica spheres are partially submerged in water. That means that the air−water interface is inside the layer; h is the immersion depth, the particle diameter is d, and distance between the particle centers is D (Figure 4). The average refractive index can be approximated by the *effective medium approach* [36] by calculating the refractive index from the volume fraction of the components and from their bulk refractive indexes. In the regular hexagonal arrangement, the volume fraction of silica at height z is

$$\alpha = \frac{2\pi}{D^2\sqrt{3}} z(d - z). \tag{5}$$

In the simplest approximation, the square of the refractive index at height z is a linear combination of those of the constituents, the square of refractive index of the particles (n_p), and that of the environment (n_e), which for water is $z < h$, and air above:

$$n(z)^2 = \alpha n_p^2 + (1 - \alpha) n_e^2. \tag{6}$$

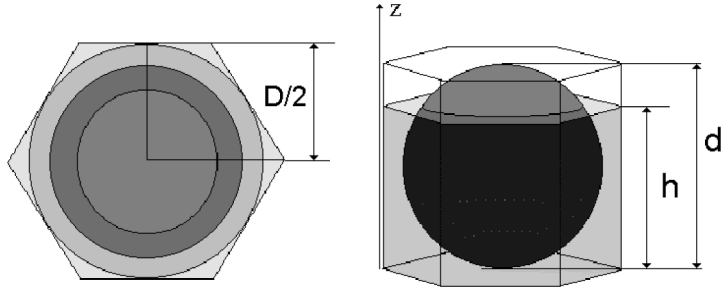

FIGURE 4 Optical model for the monolayer of spherical particles (also see the text).

We obtain the effective refractive index of the layer by averaging Equation (6) for the whole height, d:

$$n_{eff}^2 = n_a^2 + (n_w^2 - n_a^2)q + \beta^2 \frac{2\pi}{6\sqrt{3}} \left[(n_p^2 - n_a^2) - q^2(3 - 2q)(n_w^2 - n_a^2) \right]. \tag{7}$$

where n_a, n_w, and n_p are the refractive indexes of air, water, and particle, respectively, and $q = h/d$, $\beta = d/D$. Calculated effective refractive index–immersion depth curves are shown in Figure 5 for different values of β.

From the effective refractive index, the immersion depth can be approximated with the help of formula (Equation (7)). The immersion

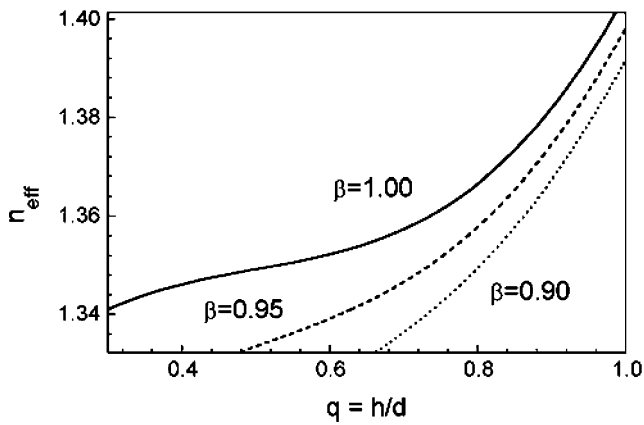

FIGURE 5 Effective refractive index (n_{eff}) as a function of the immersion (q) and packing density (β).

depth depends on the wettability of the particles, characterized by the contact angle, Θ. For spherical particles, the contact angle and the immersion, q, are related according to the formula:

$$\cos\Theta = 2q - 1. \tag{8}$$

Computer Simulation of the Surface Pressure versus Surface Area Isotherms

Once the layer was compressed beyond the collapse point and we withdrew the moving barrier and compressed the film again, the $\Pi - A$ isotherm was not reproducible. This fact points to irreversible removal of particles from the interface. We suppose that the collapse pressure (Π_c) of the layer can be associated with the contact angle of the particles. To reveal the nature of the relation, we developed a molecular dynamics computer simulation.

Implementation

A more detailed description of the implementation can be found in Agod *et al*. [29]. The simulation of the compression was performed for $N = 1000$ spherical particles in a rectangular cell with periodic boundary conditions. The size distribution could be set according to experimentally measured values. The particle−particle (p−p) interactions were derived from the experimentally gained isotherms in a manner described in the literature [37]. The compression of the layer was simulated by decreasing the area of the simulation cell by 0.5% and by rescaling the positions of the particles proportionally after every compression step. Between the steps, the layer was left to reach a local equilibrium state [29]. The surface pressure of the layer was derived from the virial theorem [38−40]:

$$\Pi = n\frac{\left\langle \sum_{i=1}^{N} m_i v_i^2 + \sum_{(i,j)} \overrightarrow{F_{ij}}\overrightarrow{r_{ij}} \right\rangle}{2N} = \frac{NkT}{A} + \frac{1}{2A}\left\langle \sum_{(i,j)} \overrightarrow{F_{ij}}\overrightarrow{r_{ij}} \right\rangle, \tag{9}$$

where $\overrightarrow{r_{ij}} = \overrightarrow{r_i} - \overrightarrow{r_j}$ is the separation between the centers of mass of particles i and j, (i,j) are the interacting pairs, $\overrightarrow{F_{ij}}$ is the force between particles i and j (derived from the interaction potential), $n = \frac{N}{A}$, v_i is the velocity of particle i, k is the Boltzmann constant and T is the ambient temperature.

In the simulation, the particles were allowed to leave the water−air interface (simply by eliminating them from the system) if their potential energy exceeded the adhesion work attributed to a single sphere

immersed in water to its equilibrium depth (Equation (1)):

$$V_i = \sum_j V_T(r_{ij}) > \gamma_{wa} R_i^2 \pi (1 - \cos(\Theta))^2, \tag{10}$$

where V_i is the potential energy of the ith particle arising from the p–p interactions (V_T). γ_{wa} is the water–air surface tension, R_i is the radius of the ith particle, and Θ is its water contact angle.

Model Materials: Stöber Silica Particles

The synthesis of silica particles by controlled hydrolysis of tetraethylorthosilicate (TEOS) in ethanol (in the presence of an aqueous solution of ammonia) has been known for more than thirty years [41]. The so-called Stöber silica has many advantageous properties for model investigations. The near-spherical, inorganic particles show narrow size distribution and are compact above a certain particle size (*ca.* 20 nm diameter) [42]. Moreover, the particles can be transferred into water from the alcoholic phase, and the hydrosol was found to be stable without any additives [43] due to a stabilizing water film between the surfaces of the particles. On the other hand, a mixture of alcosol and chloroform can be spread at the water–air interface, and the particles form a monoparticulate layer without significant loss of particles, as was shown earlier [7, 8]. The partial wetting of native Stöber silica particles can be attributed to the presence of non-hydrolyzed ethoxy groups and the "Si–O–Si" parts of the silica surface [44].

Stöber silica particles were found to form a weakly cohesive layer at the water–air interface due to the DLVO, capillary and dipole–dipole forces [37] with the secondary energy minimum at a particle–particle distance that corresponds to the contact cross-sectional area (CCSA, Figure 1) of the surface pressure–surface area isotherm. Hence, we can calculate the contact angles of particles by the traditional way (Equation (1)), integrating the isotherm from the area of CCSA.

EXPERIMENTAL

Experimental Methods, Instruments and Materials

Preparation and Characterization of Silica Particles

The alcosol of silica particles was prepared according to the Stöber method [41] by choosing appropriate reagent concentrations, 10 cm^3 tetraethyl—orthosilycate, and 10 cm^3 25% aqueous NH_3 solution in 250 cm^3 absolute ethanol, resulting in a mean particle diameter of

43 ± 5 nm. The solid content of alcosols (mg/cm^3) was determined from the amount of residual solids after solvent evaporation in a drying oven at 80°C. A JEOL JEM-100 CX II transmission electron microscope (JEOL, Peabody, MA, USA) was used to assess the particle size and shape. The samples from the layer were deposited on Formvar® film-coated carrier grids. Particle sizes were determined by measuring the diameters of (400−500) nearly spherical particles from which the particle size distribution and the sphere-equivalent mean particle diameter were determined. The mean cross section and mean volume ($\overline{V}$) of the particles for the analysis of pressure area isotherms were also calculated from the individual data [37].

Measurements

Film balance investigations. A laboratory-built and computer-controlled Wilhelmy film balance was used to determine the surface pressure (II) *versus* surface area (A) isotherms of monoparticulate layers at ambient temperature (23 ± 1°C). The sols for spreading were prepared by diluting the silica suspensions with chloroform (1 vol. alcosol + 2 vol. chloroform) then homogenizing in an ultrasonic bath for 10 min. An appropriate amount of sol was spread on the surface of the water in the film balance. After the evaporation of the spreading liquid the II-A isotherms were obtained at a rate of 3.35 cm/min of the moving barrier (corresponding to 33.2 cm^2/min). In order to assess the reproducibility, the film balance experiments were repeated five times, in most cases by spreading the same volume of the sol. The water contact angles for the characterization of the particles' surfaces were determined by using Equation (1) at different amounts of spread particles by an extrapolation method in order to take into consideration the surface pressure gradient along the layer [37, 45]. The number of spread particles (Z) was determined from the spread amount (m_{tot}) of particles in the following way:

$$Z = m_{tot}/(\rho \overline{V}), \tag{11}$$

where $\rho = 2060$ kg/m^3 [43].

Optical investigations. For the optical measurements a computer-controlled and homemade SAR instrument was used [34]. The source was a 17 mW polarized-beam HeNe laser, (Melles Griot, Carlbad, CA, USA; $\lambda = 632.8$ nm) and a PD200 silicon photodiode (Edmund Industrial Optics, Barriugtou, NI, USA) was used as a detector. The source arm and detector arm moved simultaneously, driven by a Little Step-U unipolar stepper motor (New Lynn, New Zealand). The reflected light intensity was measured around 53.1°, the Brewster

angle of water, in 0.1° or 0.05° steps. First, the reflectance curve of pure water was scanned, the layer was spread, and the moving barrier of the film balance was set to reach the desired surface pressure. Then the reflectance curve of the layer was measured. Twenty measurements were taken at each angle and the data had been averaged. The angles, averaged data, and standard deviations were stored in the measurement data file for further processing. All measurements were performed at room temperature, $T = (23 \pm 1)^{\circ}C$. In the calculations, the following refractive index values were used: 1.000 for air, 1.333 for water, and 1.450 for silica [46]. The refractive index of the silica particles was found to be between 1.43 and 1.45 [8].

Materials

For the synthesis of Stöber silica tetraethyl—orthosilycate (TEOS, >98% GC; Fluka, Buchs Sci. Switzerland), absolute ethanol (A.R., >99.7%; Reanal, Budapest, Hungary), and ammonium hydroxide (25% aqueous solution of NH_3; A.R., Reanal, Budapest, Hungary) were used as received. For the film balance experiments chloroform (>99.8% "Baker Resy Analysed," J. T. Baker Inc., Phillipsburg, NJ, USA) and distilled water (Millipore Milli Q) were used.

RESULTS

Contact Angles from the Pressure Area Isotherms

As was mentioned, the II-A isotherms were not reproducible if the samples were compressed beyond the collapse point, showing an irreversible removal of particles from the interface. Supporting this idea, whitish folds were not observed during the collapse, that—according to former observations for micron-sized particles [20]—also means the particles sank into the aqueous phase irreversibly. Hence, we could determine the advancing water contact angles from the II-A isotherms by the traditional method applying Equation (1). The contact angle, extrapolated to the mass of the particles at the position of the surface pressure sensor [37, 45], was found to be $69^{\circ} \pm 1^{\circ}$.

Contact Angles from the Computer Simulation

The simulated surface pressure *versus* surface area isotherm for an ideal case (monodisperse spheres in a hexagonal array during the whole compression) is depicted in Figure 6. The particles have the same potential energy during the compression, and hence they leave

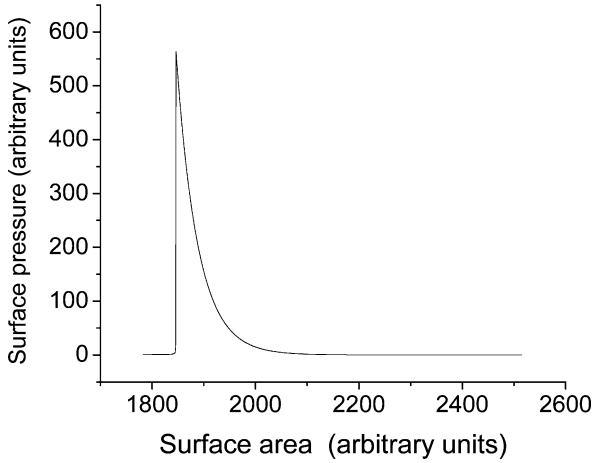

FIGURE 6 Simulated isotherm for an ideal case: monodisperse spheres with totally hexagonal ordering during the whole process.

the interface at the same time demonstrating an ideal collapse phemonenon.

Applying the real polydispersity of 43 nm spheres and scattering them randomly onto the water surface, we get a rather realistic isotherm as can be seen in Figure 7. In this case, the simulated isotherms

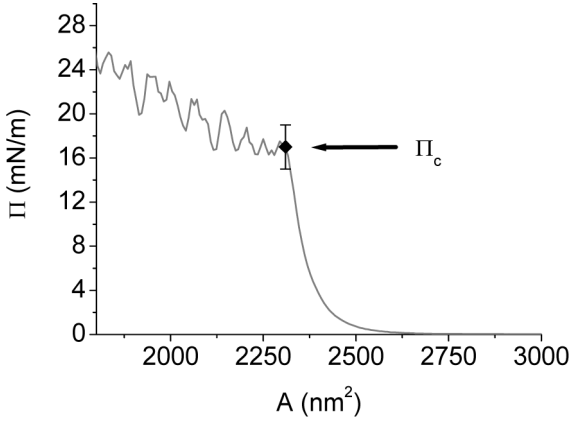

FIGURE 7 Simulated isotherm. The water contact angle of the particles was set to 37.5°.

show breakdowns similar to those of the experimentally gained isotherms. The noise of the simulated isotherm after the collapse point is due to the low number of particles ($N = 1000$) and the finite size of the compression steps. If a particle leaves the interface the others around it get more space, so the surface pressure drops and the layer expands slightly. (The aforementioned extra energy dissapation can be attributed to this relaxation process.) The experimentally gained isotherms were rising after the onset of the collapse (Figure 7), and the simulation reproduced this behavior. The increasing surface pressure of the layer after the collapse is the consequence of the different potential energy of the particles, due to the inhomogeneous layer structure, and of the polydispersity of the particles.

In real experiments the extrapolated collapse pressure was about 19 mN/m. The water contact angle of the real particles can be estimated, if we can find a simulated system where the collapse pressure corresponds to this value. In Figure 8 collapse pressures of systems with different water contact angles are presented. The collapse pressure of the simulated layer was close to the value obtained in the real experiments if the water contact angle (Θ) was set between 37.5° and 40° (Figure 8).

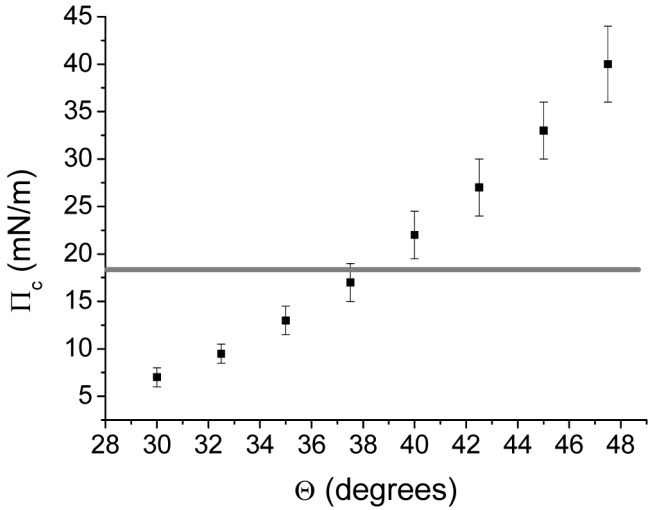

FIGURE 8 Collapse pressures (Π_c) of systems with different water contact angles (Θ). The solid line at 19.0 mN/m corresponds to the experimentally obtained collapse pressure value.

Contact Angles from the Laser-optical Investigations

It is worth mentioning that the surface pressure below the collapse pressure showed a slight decrease, keeping the surface area constant (*ca*. 0.1 *m*N/m.min) and showing the metastable state of the layer. The surface pressure drop can be attributed to the contact angle relaxation and the rearrangement of structure. No particle loss during the process was revealed; that was shown by the reproducibility of the isotherms below the collapse pressure. If we stopped the moving barrier, the surface pressure dropped. When we resumed the compression the surface pressure showed an increase during a very short time period (some seconds), and the data appeared on the same envelope (curve).

During the evaluation of the reflectance measurements, first we converted the measured intensity curves to reflectance, using the water curve for calibration [34]. The reflectance curves were evaluated with the homogeneous model by applying a Levenberg-Marquardt curve-fitting procedure [47] to fit the theoretical reflectance to the experimental data, which resulted in an effective refractive index and a layer thickness for each layer of nanoparticles. The starting value of n_{eff} was obtained from the intersection of the reflectance curve with that of the water surface (Equation (4), Figure 3). The data are summarized in Table 1, together with the particle diameters measured by means of transmisson electron microscopy (TEM). The optical thickness values agreed quite well with the TEM data, indicating that the nanoparticles produced monolayers on the water surface; in addition, the SAR method proved to be an adequate means to estimate the size of hydrophilic silica nanoparticles at the investigated particle size. The effective refractive indices were used to estimate

TABLE 1 Experimentally Obtained Parameters from the SAR Measurements and the Contact Angles Obtained by Different Methods

l (nm)	n_{eff} (refractive index)	q (h/d_{TEM})	Contact angles from different methods	d_{TEM} (nm)
41 ± 1	1.378–1.386	0.942–0.947	(*a*) 27–28° (*b*) 69–1° (*c*) 37.5–40°	43 ± 5

l: thickness of the layer; n_{eff}: effective refractive index of the layer; q: immersion; h: immersion depth of spheres; d_{TEM}: mean particle diameter (from TEM-measurements). Contact angles from SAR- (*a*), from film balance measurements (*b*), from computer simulations (*c*).

the immersion depth and the corresponding contact angles (27–28°) with the assumption that the packing density, β, was in the range of 0.91–0.96 at the steepest part of the isotherms [37] where the optical measurements were carried out. These values of packing density correspond to 2–4 nm distance between the particle surfaces [37]. The refractive index showed a slight increasing tendency when the surface layer was compressed (Table 1) in the surface pressure range of 2–12 mN/m. For comparison, we collected the contact angles obtained by different methods in Table 1.

DISCUSSION

The traditional film balance method and the computer simulation provide contact angles for the same situation, *i.e.*, at the moments of the particles' removal from the interface. The particles move toward the water phase, thus both the measured and simulated contact angles (due to the real potential energies used in the simulation) have dynamic and advancing characters, *i.e.*, they provide the maximum values of contact angles. The simulated values, in our opinion, reflect the realistic wetting properties of Stöber silica particles for the aforementioned reasons. As a first step of the collapse, the particles, due to the different particle sizes and fluctuations at the interface, should leave the interface vertically in different directions even at a lower surface pressure than its collapse value. That is, the monoparticulate film creases slightly during the compression [20, 48–49], even in the case of particles of lower hydrophobicity. An increase in the surface pressure results in more and more creased particulate film, and the particles at the water side, with the highest potential (repulsion) energy reaching the collapse pressure, begin to sink irreversibly into the water. The thickness of the layer, however (Table 1), was found to be nearly independent of the surface pressure, presumably owing to the low hydrophobicity of the particles, indicating a moderate degree of creasing. This means that the SAR provides a static and average contact angle value including the consequences of receding and advancing situations, as well. Hence, the contact angles from the SAR-measurements are in good agreement with the contact angles obtained from the simulations, also demonstrating that the traditional film balance method overestimates the contact angles in the case of low hydrophobicity particles.

Recently, there was a report about the relationship of contact angles of nanoparticles at two-liquid interfaces with ellipsometric optical parameters [50]. However, reasonable contact angles could not be obtained for the 25 nm diameter silica particles due to the complex

layer formation; it would be worth considering the application of that rigorous model calculation for our systems in the future.

CONCLUSIONS

Wettability of Stöber silica nanoparticles (*ca*. 40 nm diameter) was studied in a Wilhelmy film balance at the water–air interface. Water contact angles were determined by the traditional film balance method and by scanning angle reflectometry (SAR) of the close-packed monoparticulate layer, as well as from the analysis of the computer-simulated surface pressure versus surface area isotherms.

It was concluded that the scanning angle reflectometry provides an averaged (between the advancing and receding) static contact angle and the computer simulation gives dynamic advancing contact angles. It was shown that SAR and a combination of computer simulations with film balance measurements give consistent assessments of the contact angle of silica nanoparticles at the water–air inferface.

Moreover, it was demonstrated that the traditional film balance method, based on the whole integral of the Π-*A* isotherms, leads to erroneous contact angles even in the case of the irreversible removal of particles during the collapse. In our opinion, this finding is attributed to the continuous particle removal from the interface during the collapse that results in an extra energy dissipation. The extra energy term is related to a permanent process of the expansion and compression of the layer as a consequence of the continuous particle removal.

REFERENCES

[1] Fuerstenau, D. W. and Herrera-Urbina, R. In: Scamehorn, J. F. and Harwell, J. H. Eds., *Mineral Separation by Froth Flotation: Surfactant-Based Separation Processes*, (Marcel Dekker, New York, 1989), *Surfactant Science Series*, Vol. 33, pp. 259–319.

[2] Aveyard, R., Cooper, P., Fletcher, P. D. I., and Rutherford, C. E., *Langmuir* **9**, 604–613 (1993).

[3] Menon, V. B., Nikolov, A. D., and Wasan, D. T. J., *J. Colloid Interface Sci*. **124**(1), 317–327 (1988).

[4] Scheludko, A., Toshev, B. V., and Bojadjiev, D. T., *J.Chem. Soc. Faraday Trans*. **72**, 2815–2828 (1976).

[5] Neumann, A. W., Vargha-Butler, E. I., Hamza, H. A., and Absolom, D. R., *Colloids Surf*. **17**, 131–142 (1986).

[6] Vargha-Butler, E. I., Kashi, M., Hamza, H. A., and Neumann, A. W., *Coal Prep*. **3**, 53–75 (1986).

[7] Tolnai, Gy., Csempesz, F., Kabai-Faix, M., Kálmán, E., Keresztes, Zs., Kovács, A. L., Ramsden, J. J., and Hórvölgyi, Z., *Langmuir* **17**(9), 2683–2687 (2001).

[8] Szekeres, M., Kamalin, O., Schoonheydt, R. A., Wostyn, K., Clays, K., Persoons, A., and Dékány, I. J., *Mater. Chem.* **12**(11), 3268–3274 (2002).
[9] Szekeres, M., Kamalin, O., Grobet, P. G., Wostyn, K., Clays, K., Persoons, A., and Dékány, I., *Colloids Surf. A: Physicochem. Eng. Asp*. **227**, 77–83 (2003).
[10] Fendler, J. H., and Meldrum, F. C., *Adv. Mater*. **7**, 607–632 (1995).
[11] Garhsva, S., Contreras, S., and Goldfarb, J., *Coll. Polym. Sci*. **256**(3), 241–250 (1978).
[12] Tschajlovska, S. D. and Aleksandrova, L. B., *Chem. Technol*. **30**, 301–303 (1978).
[13] Hansford, D. T., Grant, D. J. W., and Newton, J. M., *J. Chem. Soc. Faraday Trans*. **76**, 2417–2431 (1980).
[14] Bán, S., Wolfram, E., and Rohrsetzer, S., *Colloids Surf*. **22**, 301–309 (1987).
[15] Hanning, R. N. and Rutter, P. R., *Int. J. Miner. Process*. **27**, 133–146 (1989).
[16] Diggins, D., Fokkink, L. G. J., and Ralston, J., *Colloids Surf*. **44**, 299–313 (1990).
[17] Huethorst, J. A. M. and Leenaars, A. F. M., *Colloids Surf*. **50**, 101–111 (1990).
[18] Ramesh, R. and Somasundaran, P., *J. Colloid Interface Sci*. **139**(1), 291–294 (1990).
[19] Clint, J. H. and Taylor, S. E., *Colloids Surf*. **65**, 61–67 (1992).
[20] Hórvölgyi, Z., Németh, S., and Fendler, J. H., *Langmuir* **12**(4), 997–1004 (1996).
[21] Yang, Y.-W., Zografi, G., and Miller, E. E., *J. Colloid Interface Sci*. **122**(1), 24–34 (1988).
[22] Yang, Y.-W., Zografi, G., and Miller, E. E., *J. Colloid Interface Sci*. **122**(1), 35–46 (1988).
[23] Crawford, R., Koopal, L. K., and Ralston, J., *Colloids Surf*. **27**, 57–64 (1987).
[24] Hadjiiski, A., Dimova, R., Denkov, N. D., Ivanov, I. B., and Borwankar, R., *Langmuir* **12**, 6665–6675 (1996).
[25] Aveyard, R., Binks, B. P., Fletcher, P. D. I., and Rutherford, C. E., *Colloids Surf. A: Physicochem. Eng. Asp*. **83**, 89–98 (1994).
[26] Paunov, V. N., *Langmuir* **19**(19), 7970–7976 (2003).
[27] Clint, J. H. and Quirke, N., *Colloids Surf. A: Physicochem. Eng. Asp*. **78**, 277–278 (1993).
[28] Hórvölgyi, Z., Máté, M., Dániel, A., and Szalma, J., *Colloids Surf. A: Physicochem. Eng. Asp*. **156**, 501–508 (1999).
[29] Agod, A., Tolnai, Gy., Esmail, N., and Hórvölgyi, Z., *Prog. Colloid Polymer Sci*. **125**, 54–60 (2004).
[30] Schaaf, P., Déjardin, P., and Schmitt, A., *Langmuir* **3**, 1131–1135 (1987).
[31] Mann, E. K., van der Zeeuw, E. A., Koper, G. J. M., Schaaf, P., and Bedeaux, D., *J. Phys. Chem*. **99**, 790–797 (1995).
[32] van der Zeeuw, E. A., Sagis, L. M., Koper, G. J. M., Mann, E. K., Haarmans, M. T., and Bedeaux, D., *J. Chem. Phys*. **105**, 1646–1653 (1996).
[33] Mann, E. K., Heinrich, L., Voegel, J. C. and Schaaf, P., *J. Chem. Phys*. **105**, 6082–6085 (1996).
[34] Hild, E., Seszták, T., Völgyes, D., and Hórvölgyi, Z., *Prog. Colloid. Polymer Sci*. **125**, 61–67 (2004).
[35] Hórvölgyi, Z., Agod, A., Hild, E., Kálmán, E., and Tolnai, Gy. In: XVIIth Conference of the European Colloid and Interface Society, Florence, Italy, (2003), Abstr. OR5/12, p. 120.
[36] Boyd, R. V., Gehr, R. J., Fischer, G. L., and Sipe, J. E., *Pure Appl. Opt*. **5**, 505–511 (1996).
[37] Tolnai, Gy., Agod, A., Kabai-Faix, M., Kovács, A. L., Ramsden, J. J., and Hórvölgyi, Z., *J. Phys. Chem. B*, **107**, 11109–11116 (2003).
[38] Rapaport, D.C. *The Art of Molecular Dynamics Simulation* (Cambridge University Press, Cambridge, 1995).

[39] Sun, J. and Stirner, T., *Langmuir* **17**, 3103–3108 (2001).
[40] Fenwick, N. I. D., Bresme, F., and Quirke, N., *J. Chem. Phys*. **114**(16), 7274–7282 (2001).
[41] Stöber, W., Fink, A., and Bohn, E., *J. Colloid Interface Sci*. **26**, 62–69 (1968).
[42] Bailey, J. K. and Mecartney, M. L., *Colloids Surf.* **63**, 131–138 (1992).
[43] Kabai-Faix, M., *Magy. Kem. Foly*. **102**(1), 33–41 (1996).
[44] Suratwala, T. I., Hanna, M. L., Miller, E. L., Whitman, P. K., Thomas, I. M., Ehrmann, P. R., Maxwell, R. S., and Burnham, A. K., *J. Non-Crystalline Solids* **316**, 349–363 (2003).
[45] Máté, M., Fendler, J. H., Ramsden, J. J., Szalma, J., and Hórvölgyi, Z., *Langmuir* **14**, 6501–6504 (1998).
[46] Perry, L. H. *Chemical Engineers' Handbook (in Hungarian)* (Műszaki Könyvkiadó, Budapest, 1968).
[47] Press, W. H., Teukolsky, S. A., Vetterling, W. T., and Flannery, B. P. *Numerical Recipes in C, The Art of Scientific Computing* (Cambridge University Press, New York, 1988).
[48] Aveyard, R., Clint, J. H., Nees, D., and Paunov, V. N., *Langmuir* **16**, 1969–1979 (2000).
[49] Aveyard, R., Clint, J. H., Nees, D., and Quirke, N., *Langmuir* **16**, 8820–8828 (2000).
[50] Binks, B. P., Clint, J. H., Dyab, A. K. F., Fletcher, P. D. I., Kirkland, M., and Whitby, P., *Langmuir* **19**, 8888–8893 (2003).